

# 3D interacting magnetic multilayered nanowire arrays: the emergence and evolution of new first-order reversal curve features

A Ghafouri<sup>1</sup>, A Ramazani<sup>1,2</sup>  and A H Montazeri<sup>1</sup> 

<sup>1</sup> Institute of Nanoscience and Nanotechnology, University of Kashan, Kashan 87317–51167, Iran

<sup>2</sup> Department of Physics, University of Kashan, Kashan 87317–51167, Iran

E-mail: [rmzn@kashanu.ac.ir](mailto:rmzn@kashanu.ac.ir)

Received 30 June 2019, revised 1 December 2019

Accepted for publication 17 December 2019

Published 9 January 2020



## Abstract

The crucial role of magnetostatic interactions in tuning properties of storage devices based on magnetic nanowires (NWs) has recently been highlighted by advanced characterization techniques including the first-order reversal curve (FORC) analysis, evaluating physical entities constituting conventional 2D NW systems. Herein, FORC diagrams of ferromagnetic (FM)/non-magnetic (NM) multilayered NW arrays are simulated using Monte Carlo calculations, involving magnetostatic interactions between segments in 3D space. The FM length is constant to 6  $\mu\text{m}$  whereas the NM length ( $L_{\text{NM}}$ ) varies from 10 to 300 nm, significantly influencing interwire and intrasegment interactions of neighboring NWs and coupled segments along the NW length. Intriguingly, this is accompanied with the emergence of two new FORC diagram features in addition to the typical demagnetizing-type feature, indicating complex behavior of the 3D interacting NWs with the same anisotropy field for each FM segment. The FORC coercivity of the emerging features is tracked individually, presenting evolution as a function of  $L_{\text{NM}}$ . Our results also evidence an increase in interwire and intrasegment interactions when increasing NW diameter, being in accordance with total magnetostatic energy calculations.

**Keywords:** multilayered nanowire arrays, Monte Carlo simulation, first-order reversal curve, magnetic features, total magnetostatic energy, 3D interactions

(Some figures may appear in colour only in the online journal)

## Abbreviations

FM	Ferromagnetic
NM	Non-magnetic
NW	Nanowire
FORC	First-order reversal curve
$L_{\text{FM}}$	FM length
$L_{\text{NM}}$	NM length
$D$	Diameter
$d$	Interwire distance
$H_{\text{c}}^{\text{FORC}}$	FORC coercivity
$E_{\text{tot}}$	Total magnetostatic energy

## 1. Introduction

After the discovery of the giant magnetoresistance (GMR) effect in 1988 [1], spintronics has flourished and provided advances in high-density magnetic storage and low-power processing of digital information based on the electron spins [2–6]. The GMR effect is also exploited for extremely sensitive magnetic field detectors and data read heads consisting of ferromagnetic (FM) layers separated by non-magnetic (NM) layers [7, 8]. For the past decades, progress in spintronics research area has significantly relied on the monumental decreases in size of GMR structures and focused on artificially

structured materials, thus acting as a key in the development of portable electronic devices and causing a breakthrough in modern high-density disk drivers [9–11].

In this regard, recent developments in lithography processes, deposition techniques and theoretical understanding of nanoscale materials have realized the necessity of investigating their magnetic behavior with a high level of accuracy [11]. Particularly, cylindrical multilayered nanowire (NW) arrays have shown practical applications exploiting the GMR effect [12–14] while also suggesting potential uses in three-dimensional (3D) data storage devices [15–17]. From an experimental standpoint, arrays of multilayered NWs with tunable morphology and hexagonal ordering can be easily fabricated using template-based electrochemical deposition approaches [18–20]. Previous experimental and theoretical investigations have revealed the dependency of the multilayered NW magnetic properties on their material type, segment morphology including FM length ( $L_{\text{FM}}$ ), NM spacer length ( $L_{\text{NM}}$ ) and diameter ( $D$ ) [21–23].

For read operations in nanoscale hard drives, it is vital to have media with high signal output and low noise [24]. The latter features magnetostatic interactions between segments and inter-segment coupling between FM segments along the NW length (or intrasegment coupling) so that the NM metallic spacer in multilayered NWs may play a significant role in determining the overall magnetic characteristics [21, 25].

The involvement of magnetostatic interactions becomes increasingly important and effective in 3D storage devices compared with conventional two-dimensional (2D) ones [16, 25–28]. Accordingly, understanding the effect of magnetostatic interactions occurring between segments may pave the way for future research on high-speed and efficient 3D storage devices, and tuning their magnetic properties. In this direction, Rando and Allende [29] developed a numerical analysis of magnetization reversal processes in magnetostatically interacting 180 nm diameter Ni/NM metallic spacer (e.g. Cu) NW arrays with Ni segment numbers ranging from 1 to 13 along the NW length and different spacer lengths (ranging from 10 to 1000 nm). Using Monte Carlo simulation, they calculated corresponding hysteresis loops (involving different nucleation and annihilation fields), and found that the nucleation fields increased when increasing the segment number or decreasing the spacer length [29]. Moreover, depending on the reversal mode, annihilation fields showed non-monotonic behaviors.

As extensively discussed in the literature [30, 31], hysteresis loop measurements and calculations provide information only on the average magnetic behavior. For this reason, advanced characterization methods such as first-order reversal curve (FORC) analysis are employed to investigate details of magnetic domains, coercive field distribution and interaction field distribution [25, 27, 32–36]. Notwithstanding, while FORC diagrams of experimentally fabricated multilayered NWs (e.g., Fe/Cu [21], Co/Cu [37] and Ni/Cu [25] NWs) with different segment sizes have been considerably investigated in previous investigations, less attention has been paid to numerically simulate and study their FORC analysis. Importantly,

simulated calculations may clarify the correlation between FORC distributions and physical entities constituting the nanoscale magnetic system [31, 38, 39]. In this respect, using a mean-field approach, Ruta *et al* [40] have recently shown the influence of magnetostatic interactions on intrinsic switching field distribution of magnetic particles so that the FORC analysis is found to be highly accurate for magnetic systems with weakly correlated interactions. In addition, Gilbert *et al* [41] numerically investigated coercive field distributions in interacting 2D Co nanomagnet arrays, and the FORC analysis enabled them to extract quantitative information about magnetizing- and demagnetizing-type interactions observed in experimental FORC diagrams. They also found that magnetic interaction changes can shift coercive field distributions, thus tilting the ridge and inducing an edge feature in the resulting FORC diagrams of 2D nanomagnet arrays [41].

In this paper, FORC diagrams of 3D arrays of magnetic multilayered NWs with variable  $L_{\text{NM}}$ ,  $D$  and interwire distance ( $d$ ) are numerically investigated using Monte Carlo simulation calculations. Especially, the influence of magnetizing- (*intrasegment*) and demagnetizing-type (*interwire*) magnetostatic interactions on magnetic phases and coercive field distributions of the multilayered NWs is comprehensively studied. This study reveals new emerging FORC diagrams in the 3D multilayered NWs with no precedent in the literature, which could be evolved and taken into consideration when designing advanced spintronic devices in a foreseeable future.

## 2. Numerical model

### 2.1. Simulation of the FORC diagram

Since 1999 when it was employed by Pike *et al* [42] as a powerful method of investigating hysteresis in magnetic systems, the FORC diagram made of contour plots of a 2D distribution function has been extensively used to qualitatively and quantitatively identify and distinguish between constituents of nanoscale structures. The FORC diagram analysis is based on the mathematical Preisach model of interacting hysterons created from square hysteresis loops with a critical field  $H_c$  and an interaction field  $H_u$  [34, 42]. In the case of NW arrays magnetically saturated in the parallel direction to the NW axis, the hysterons may provide physical interpretations on  $H_c$  and  $H_u$ , tracking switching and interaction fields acting on individual NWs [27, 30, 34]. While the NW magnetic moment is in ‘up’ or ‘down’ state, and the intrinsic coercive field of each NW varies as a function of its composition or morphology, changing interactions can affect switching events occurring in NW arrays [31]. Thus, interwire and intrasegment interactions in the complex case of 3D multilayered NWs may play key roles in determining FORC distributions [25].

To simulate FORC diagrams, the multilayered NW system was initially saturated by applying a positive magnetic field  $H_{\text{Sat}}$  parallel to the NW axis, and then reducing the magnetic field to a reversal field  $H_r$ . By sweeping  $H_r$  back to  $H_{\text{Sat}}$  while measuring magnetization  $M(H, H_r)$ , a FORC resulted.

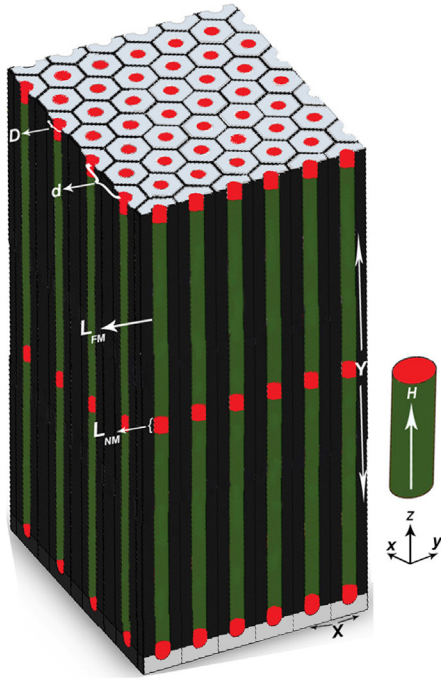


**Figure 1.** Schematic illustration and simulation parameters of 3D multilayered NW arrays embedded in a hexagonally ordered anodic aluminum oxide template.

This process was repeated until a series of FORCs was obtained. The  $H_{\text{Sat}}$  was ranged from  $\pm 500$  Oe to  $\pm 2000$  Oe, saturating different NWs with different morphological characteristics. A step number of 100 was also chosen to obtain high resolution FORC diagrams. The FORC distribution function ( $\rho_{\text{FORC}}$ ) providing information about all NW system's hysterons was then defined as follows [34]:

$$\rho_{\text{FORC}}(H, H_r) = -\frac{1}{2} \frac{\partial^2 M(H, H_r)}{\partial H \partial H_r}. \quad (1)$$

When evaluating  $\rho_{\text{FORC}}$ , data points were plotted on a spaced square grid in the  $\{H, H_r\}$  coordinate system whose number of points on the local grid was  $[2 \times (\text{Smoothing Factor}) + 1]^2$  with the point  $P$  at the center. Notably, the Smoothing Factor was set to 2 in the calculations [43]. The following polynomial surface was taken into account when fitting the  $M(H, H_r)$  of the data points on it [42]:

$$M(H, H_r) = a_1 + a_2 H + a_3 H^2 + a_4 H_r + a_5 H_r^2 + a_6 H H_r \quad (2)$$

in which  $-a_6$  value represented  $\rho_{\text{FORC}}$  at  $P$ . As a 2D contour plot, the FORC diagram ranged from blue (minimum  $\rho_{\text{FORC}}$ ) to red (maximum  $\rho_{\text{FORC}}$ ) color. For convenience, the coordinates  $\{H, H_r\}$  also changed to  $45^\circ$  rotated  $H_c$  and  $H_u$  axes as given below:

$$H_c = \frac{H - H_r}{2}, \quad H_u = \frac{H + H_r}{2}. \quad (3)$$

## 2.2. 3D multilayered NW system

As schematically illustrated in figure 1, 3D multilayered NW arrays were theoretically embedded in a hexagonally ordered anodic aluminum oxide template ( $200\text{--}500 \mu\text{m}^2$  in surface area) with nanopore diameters and interpore distances ranging from  $D = 180$  to  $300$  nm and  $d = 500$  to  $1000$  nm, respectively. Experimentally, it is possible to fabricate aluminum oxide templates with  $D \sim 180$  nm (as-prepared template) to  $300$  nm (by widening the pores) along with  $d = 500$  nm using the anodization process in phosphoric acid [44]. However,  $d$  increased up to  $1000$  nm to investigation the evolution of FORC features.

The total number of individual cylindrical multilayered NWs was set to 4096. In this respect, each NW comprised 11 ferromagnetic segments with a length of  $L_{\text{FM}} = 6 \mu\text{m}$  separated by 10 non-magnetic segments (as spacers) with variable lengths ranging from  $L_{\text{NM}} = 10$  to  $300$  nm. Thereby, the effects of  $L_{\text{NM}}$ ,  $D$ ,  $d$  on the FORC diagrams of the 3D multilayered NW arrays were studied using Monte Carlo simulation. The multilayered NWs with up and down magnetic states along the  $z$  direction, and an internal energy  $E_{\text{tot}}$  (as given below) were submitted to magnetostatic interactions [45]:

$$E_{\text{tot}} = E_{\text{Zeeman}} + E_{\text{Ani}} + E_{\text{Mag}} \quad (4)$$

in which  $E_{\text{Zeeman}}$ ,  $E_{\text{Ani}}$  and  $E_{\text{Mag}}$  are related to the external magnetic field applied in the  $z$  direction ( $H_{\text{App}}$ ), the magnetic shape anisotropy of each FM segment and the internal magnetostatic energy, respectively.  $E_{\text{Zeeman}}$  and  $E_{\text{Ani}}$  are obtained according to equations (5) and (6) [29, 45]:

$$E_{\text{Zeeman}} = -\vec{\mu} \cdot \vec{H}_{\text{App}} = -\mu_0 M_0 V \sum_{m=1}^N \vec{\delta}_m \cdot \vec{H}_{\text{App}} \quad (5)$$

$$E_{\text{Ani}} = -\vec{\mu} \cdot \vec{H}_{\text{Ani}} = -\mu_0 M_0 V \sum_{m=1}^N \vec{\delta}_m \cdot \vec{H}_{\text{Ani}} \quad (6)$$

where  $\mu_0$ ,  $M_0$ ,  $V$  and  $\vec{\delta}_m$  are the vacuum permeability, saturation magnetization, volume of the FM segment and the stable magnetic states around the  $z$  direction, respectively.

The dipolar interaction energy between two magnetic NWs is obtained as follows [46]:

$$E_{\text{int}}(m, n) = 2\delta_m \delta_n \int_0^\infty \frac{dq}{q^2} J_0\left(\frac{qd}{L_{\text{FM}}}\right) J_1^2\left(\frac{qD}{2L_{\text{FM}}}\right) (1 - e^{-q}) \quad (7)$$

where  $\delta_m$  and  $\delta_n$  are indicative of the magnetic states (up and down) along the  $z$  direction.  $J$  is the Bessel function and  $q$  is the Bessel function parameter. Moreover,  $d$ ,  $D$  and  $L_{\text{FM}}$  are the interwire distance, NW diameter and FM segment length, respectively. The equation (7) allows for writing  $E_{\text{int}}(m, n)$  as:  $E_{\text{int}}(m, n) = \delta_m \delta_n E_{\text{int}}(d)$  so that  $\delta_m \delta_n = 1$  if  $\delta_m = \delta_n$ , and  $\delta_m \delta_n = -1$  if  $\delta_m \neq \delta_n$ . In principle, equation (7) should be solved numerically. Nevertheless, for  $L_{\text{FM}}/D \gg 1$ , it is possible to expand the Bessel function  $J_1$  as follows [46]:

$$J_1(a) = \frac{a}{2} - \frac{a^3}{16} + \sum_{\alpha=1}^{\infty} \frac{(-1)^\alpha}{\alpha! \Gamma(\alpha+2)} \left(\frac{a}{2}\right)^\alpha. \quad (8)$$

Accordingly, one can approximate equation (5) by:

$$E_{\text{int}}^\beta(d) = \frac{D^2}{8L_{\text{FM}}d} \sum_{\beta=1}^{\infty} p_\beta \quad (9)$$

where  $\beta$  defines the order of the expansion. By considering the first term in the sum, one can write:

$$p_1 = 1 - \frac{1}{\beta_1} \quad (10)$$

in which  $\beta_1 \equiv \frac{\sqrt{d^2 + L_{\text{FM}}^2}}{d}$ . Overall,  $E_{\text{Mag}}$  for an array of magnetic NWs is obtained as follows:

$$E_{\text{Mag}} = -\vec{\mu} \cdot \vec{H}_{\text{Mag}} = -\frac{\mu_0 M_0^2 D^2}{32 L_{\text{FM}}} v \sum_{m=1}^N \sum_{\substack{n=1 \\ n \neq m}}^N \left( \frac{1}{\sqrt{X^2 + (L_{\text{FM}} + Y)^2}} - \frac{2}{\sqrt{X^2 + Y^2}} + \frac{1}{\sqrt{X^2 + (L_{\text{FM}} - Y)^2}} \right) \vec{\delta}_m \cdot \vec{\delta}_n \quad (11)$$

where  $N$  is the total number of segments,  $X$  is the distance between two NWs, and  $Y$  is the distance between two FM segments (see figure 1). In this study,  $H_{\text{Ani}} = 228$  Oe and  $M_0 = 480$  emu cm<sup>-3</sup> (corresponding to the element Ni) were taken into consideration [29, 47].

It should be noted that, once a magnetic moment was flipped, the  $H_{\text{Ani}}$  associated with the moment was also reverted. In other words,  $\delta_m$  was arbitrarily oriented in the new magnetic state with a probability,  $P$ , as follows:  $P = \min [1, \exp(-\Delta E/k_B T)]$  in which  $\Delta E$  is the energy change arising from  $\delta_m$  reorientation, and  $k_B$  is the Boltzmann constant. Accordingly,  $H_{\text{Ani}}$  would change to  $-H_{\text{Ani}}$  when reverting the magnetization i.e. changing  $\delta_m$  to  $\delta_n$ . This is because the magnetic state newly occurred in the NW system would be stable. Using Metropolis algorithm, Monte Carlo simulations were performed at the temperature of zero Kelvin since the heating was not able to provide enough energy to switch magnetic moments of the multilayered NW system. Under such condition, the first realization of Monte Carlo simulation was continued until the NW system became stable, and then another realization started. Notably, the number of independent realizations needed to stabilize the system was set to a maximum of 20000. Such amount of realization could be credible since the FORC step was small and precise enough. However, the conditions applied were set to reach stabilization. The FORC diagrams were obtained by sequential procedure. Note that, the magnetization direction of all segments was initially parallel to the magnetic field, and each segment was in the minimum energy. The magnetic field was then reduced by one step for all segments while also applying the minimum energy condition for each segment with flipping magnetization using the Metropolis algorithm. This procedure was repeated for all segments until the NW system reached the minimum energy.

In other words, there was no possibility of the magnetization flipping for each segment after reaching the minimum energy. The precision of the energy minimization was controlled by reducing the magnetic field step so that the simulation was checked for different field steps to obtain the optimum step value.

In addition, due to the large enough  $L_{\text{NM}} (\geq 10 \text{ nm})$ , exchange interactions and Ruderman–Kittel–Kasuya–Yosida interactions between the FM segments were ignored.

### 3. Results and discussion

Using Monte Carlo calculations, arrays of interacting 3D FM/NM multilayered NWs with variable  $L_{\text{NM}}$  (ranged between

10 and 300 nm),  $D$  (180–300 nm) and  $d$  (500–1000 nm) were simulated, according to section 2.2. The effects of  $L_{\text{NM}}$ ,  $D$  and  $d$  on simulated FORC diagrams of the NWs are presented and compared in the following sections.

#### 3.1. The effect of NM spacer length ( $L_{\text{NM}}$ ) on FORC diagrams

Figures 2(a)–(i) show FORC diagrams of 3D FM/NM multilayered NWs with  $L_{\text{NM}} = 10, 30, 60, 80, 100, 150, 200, 250$  and 300 nm, respectively, having constant  $D = 180$  nm and  $d = 500$  nm. From figure 2(a), a broad FORC distribution elongated along the  $H_u$  axis is found, being proportional to the demagnetizing-type interwire interactions ( $\Delta H_u$ ) in parallel saturation [26] ranged between  $\Delta H_u = \pm 1200$  Oe. In this case, the multilayered NWs have a very similar coercivity with a narrow distribution width, which can be extracted from the FORC diagram.

Figure 3 shows that the respective irreversible FORC coercivity ( $H_c^{\text{FORC}}$ ) of the interacting FM/NM NWs with  $L_{\text{NM}} = 10$  nm,  $D = 180$  nm and  $d = 500$  nm is obtained to be 420 Oe (in black). Taking into account a perfect coherent magnetization rotation based on the Stoner–Wohlfarth model [45], the coercivity of each FM segment with high-aspect-ratio ( $>10$ ) is expected to be equal to  $H_{\text{Ani}}$ . Therefore, the considerable difference between the  $H_{\text{Ani}}$  (220 Oe) and  $H_c^{\text{FORC}}$  (420 Oe) of the multilayered NW arrays (having FM segment aspect ratios larger than 30) may be caused by the effective interwire and intrasegment interactions of neighboring NWs and coupled segments along the NW length, respectively. While the former can be directly manifested in the interaction field distribution along the  $H_u$  axis of the FORC diagram due to its demagnetizing-type nature [21, 25, 27], the latter can indirectly influence the magnetostatic interactions.



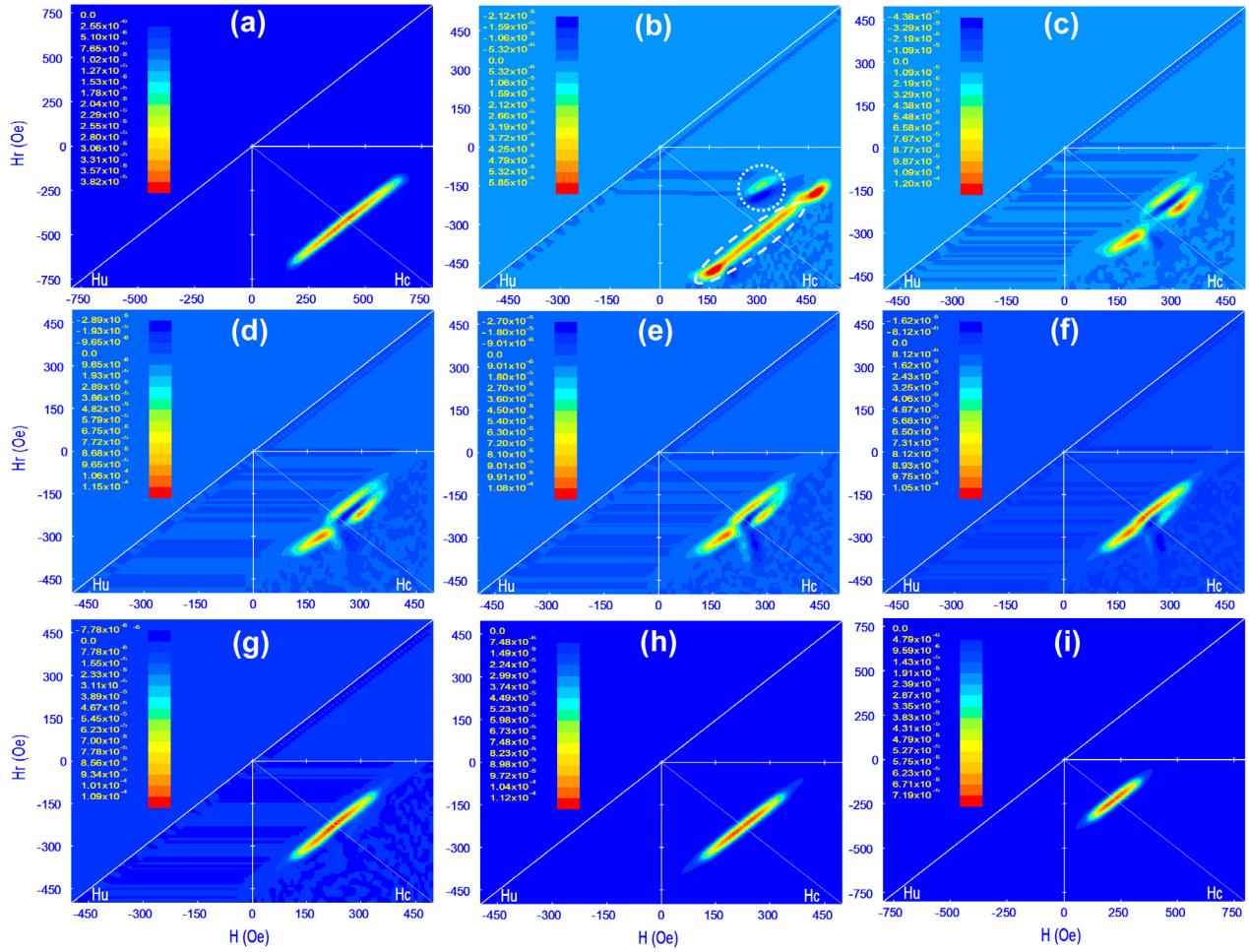


**Figure 2.** FORC diagrams of FM/NM multilayered NWs with constant  $D = 180$  nm and  $d = 500$  nm, and variable  $L_{NM}$  of: (a) 10 nm, (b) 30 nm, (c) 60 nm, (d) 80 nm, (e) 100 nm, (f) 150 nm, (g) 200 nm, (h) 250 nm and (i) 300 nm. The dashed circle and oval in panel (b) mark the first and second features appearing in the FORC diagrams, respectively.

By increasing  $L_{NM}$  from 10 to 20 nm,  $H_c^{FORC}$  sharply decreases from 420 to 320 Oe (see figure 3), and is accompanied with a reduction in  $\Delta H_u$  from 1200 to 800 Oe. In other words, the increase in Cu spacer length leads to a decrease in the magnetizing-type intrasegment interactions between FM segments. In turn, this decrease manifests itself as a reduction in the  $\Delta H_u$  of the FORC diagram (not shown here). Interestingly, further increasing  $L_{NM}$  to 30 nm leads to the formation of two new FORC features in the corresponding diagram, according to figure 2(b). The first feature, marked with a dashed circle, is a pair distribution with positive and negative FORC peaks. The corresponding positive  $H_c^{FORC}$  is extracted and presented in figure 3 (in green).

As can be seen,  $H_c^{FORC} = 230$  Oe is almost equal to  $H_{Ani}$  of each FM segment. The second feature, marked with a dashed oval, has a sharp and localized positive peak alongside the typical FORC distribution observed for  $L_{NM} < 30$  nm. In this way,  $H_c^{FORC}$  of the second feature (shown in figure 3 in red) is found to be very close ( $\sim 320$  Oe) to that of the typical feature of FM/NM multilayered NWs with  $L_{NM} = 30$  nm. Generally

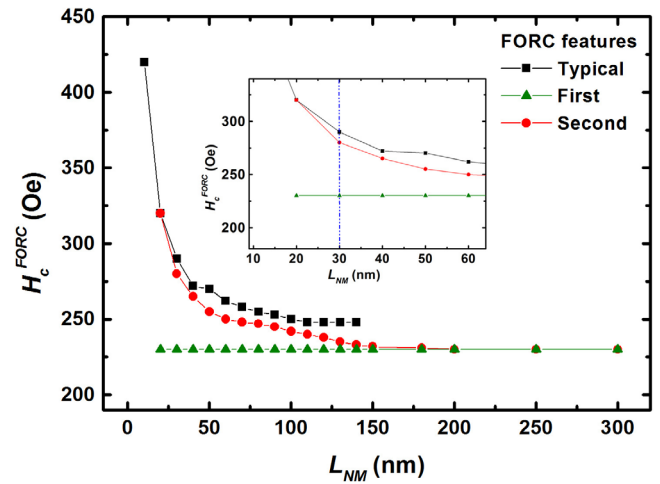


**Figure 3.** Irreversible FORC coercivity ( $H_c^{FORC}$ ) of interacting FM/NM multilayered NWs as a function of  $L_{NM}$  for  $D = 180$  nm and  $d = 500$  nm. The inset highlights the separation of the second feature from the typical one.

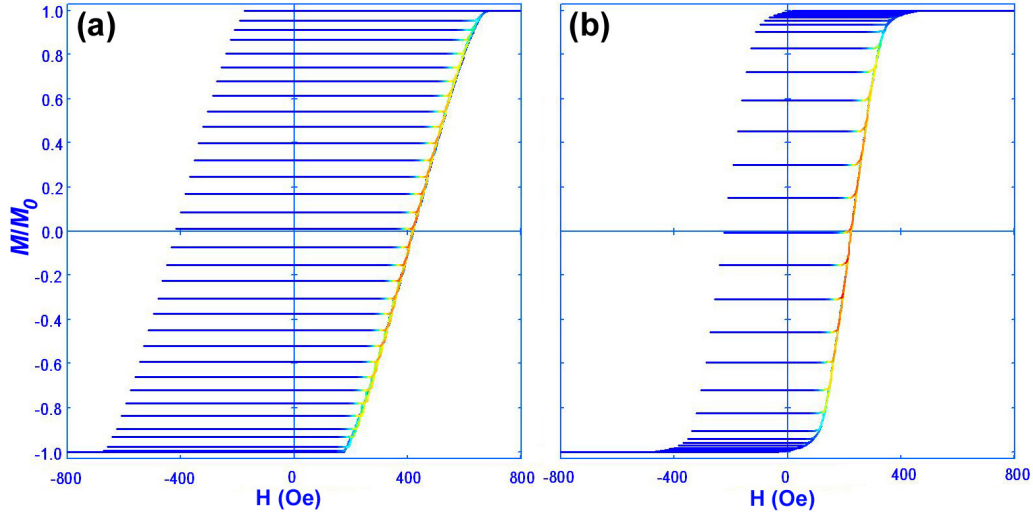


**Figure 4.** FORC diagrams in hysteresis loops for FM/NM multilayered NWs with  $L_{\text{NM}}$  of: (a) 10 nm and (b) 300 nm at constant  $D = 180$  nm and  $d = 500$  nm. Note: the color scale (ranged from blue (minimum  $\rho_{\text{FORC}}$ ) to red (maximum  $\rho_{\text{FORC}}$ )) in parts (a) and (b) is the same as that of parts (a) and (i) in figure 2, respectively.

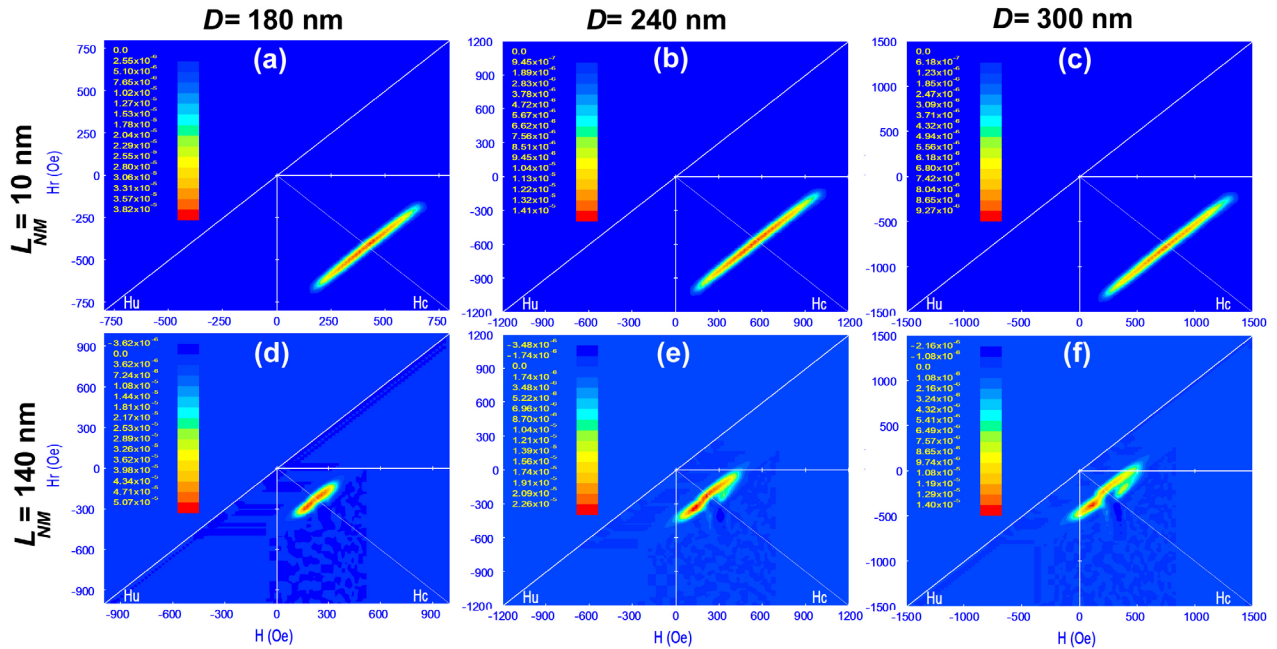


**Figure 5.** FORC diagrams of FM/NM multilayered NWs with constant  $d = 500$  nm and variable  $D = 180$ – $300$  nm for (a)–(c)  $L_{\text{NM}} = 10$  nm and (d)–(f)  $L_{\text{NM}} = 140$  nm. Note: magnitude of the magnetic field  $H$  is different for FORC diagrams in each row.

speaking, it is inferred that, while  $H_{\text{Ani}}$  of the FM segments is the same in the simulations, the reduced intrasegment interactions (arising from the increase in  $L_{\text{NM}}$ ) induce complex features of coercive field distributions in the FORC diagram.

From figures 2(b)–(d), increasing  $L_{\text{NM}}$  from 30 to 80 nm reduces the FORC intensity of the typical feature while remaining its respective  $H_{\text{c}}^{\text{FORC}}$  constant to 255 Oe. Concurrently, location of the second feature separates from the typical one and nears the first feature. In this case, the corresponding  $H_{\text{c}}^{\text{FORC}}$  of the typical and second features shows a decreasing trend from 290 to 255 Oe and 280 to 245 Oe, respectively. For  $80 < L_{\text{NM}}$  (nm)  $\leq 140$ , while  $H_{\text{c}}^{\text{FORC}}$  of

the typical features remains constant between 245–255 Oe,  $H_{\text{c}}^{\text{FORC}}$  of the second features further approaches that of the first feature (see figures 2(b)–(f) and 3). For  $L_{\text{NM}} > 140$  nm, the typical feature completely disappears in the diagrams and the first feature dominates the FORC distribution of FM/NM multilayered NW arrays.

By comparing between  $\Delta H_{\text{u}}$  values for  $L_{\text{NM}} = 10$  nm ( $\Delta H_{\text{u}} = 1200$  Oe) and 300 nm ( $\Delta H_{\text{u}} = 720$  Oe) (figures 2(a) and (i)), it is indicated that the magnetizing-type intrasegment interactions arising from the typical feature are considerably higher than those from the first feature. Therefore, the decoupling between the FM segments reduces the magnetostatic

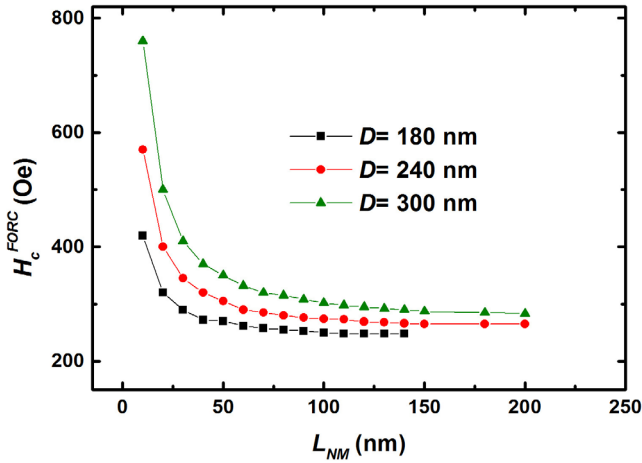


**Figure 6.** The comparison between  $H_c^{\text{FORC}}$  values (extracted from typical FORC distribution) of FM/NM multilayered NWs as a function of  $L_{\text{NM}}$  for  $D = 180, 240$  and  $300$  nm at  $d = 500$  nm.

**Table 1.**  $H_c^{\text{FORC}}$  values (extracted from typical FORC distribution) of FM/NM multilayered NWs for different  $L_{\text{NM}}$  and  $D$  at  $d = 500$  nm.

	$D = 180$ nm	$D = 240$ nm	$D = 300$ nm
$L_{\text{NM}}$ (nm)	$H_c^{\text{FORC}}$ (Oe)	$H_c^{\text{FORC}}$ (Oe)	$H_c^{\text{FORC}}$ (Oe)
10	420	570	760
30	290	345	410
60	262	290	332
80	255	280	315
100	250	275	302
120	248	269	295
140	245	266	290
150	—	265	287
180	—	265	285
200	—	265	283

interactions from neighboring NWs. It also causes multilayered NW arrays to have very similar coercivity, being comparable to  $H_{\text{Ani}}$  of each segment.

FORC diagrams in hysteresis loops for FM/NM multilayered NWs with  $L_{\text{NM}}$  of 10 nm and 300 nm are depicted in figures 4(a) and (b), respectively. The colored hysteresis loops evidently show the different coercive fields and  $\Delta H_u$  values for  $L_{\text{NM}}$  of 10 nm and 300 nm.

### 3.2. The effect of NW diameter ( $D$ ) on FORC distribution

Figures 5(a)–(f) show FORC diagrams of FM/NM multilayered NWs with constant  $d = 500$  and variable  $D = 180$ – $300$  nm for  $L_{\text{NM}}$  of 10 and 140 nm, respectively. At  $L_{\text{NM}} = 10$  nm, increasing  $D$  perceptibly pushes the typical FORC distribution toward higher coercive fields while also broadening  $\Delta H_u$ . Alternatively, at  $L_{\text{NM}} = 140$  nm, the typical FORC distribution pushes back toward the first FORC feature, regardless of  $D$  value. For better clarity, figure 6 shows

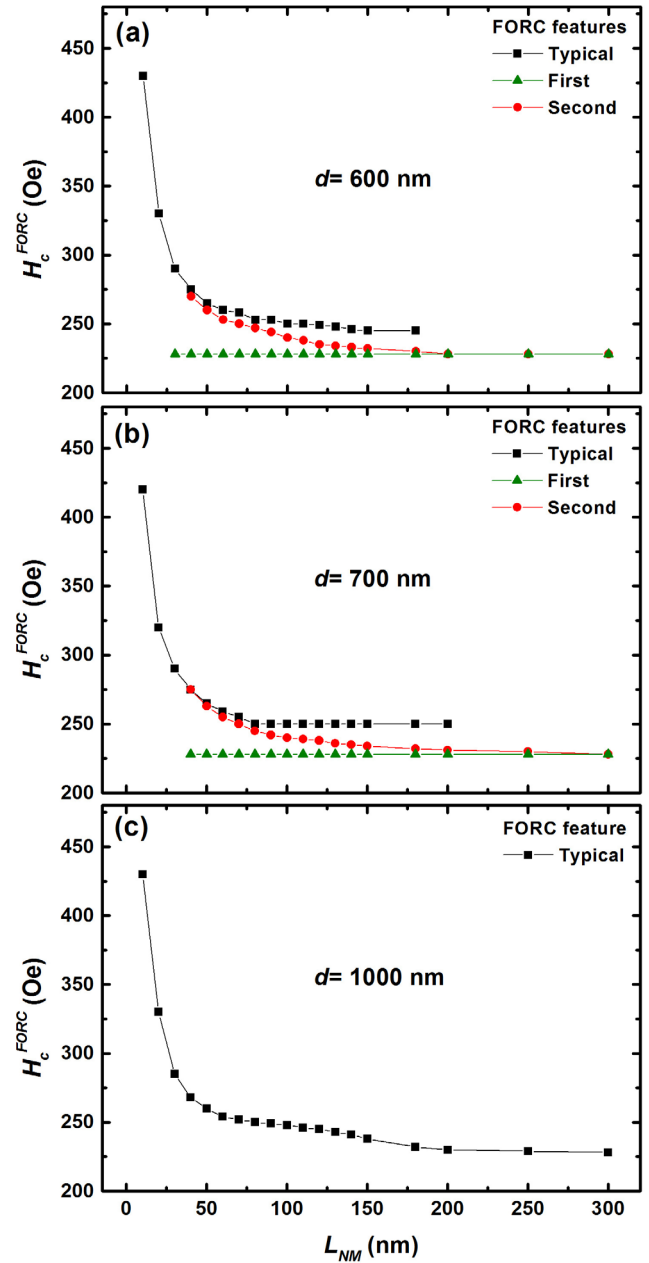


**Figure 7.**  $H_c^{\text{FORC}}$  of FM/NM multilayered NWs as a function of  $L_{\text{NM}}$  for different  $d$  of: (a) 600 nm, (b) 700 nm and (c) 1000 nm at  $D = 180$  nm.

the comparison between  $H_c^{\text{FORC}}$  (extracted from the typical FORC distribution) as a function of  $L_{\text{NM}}$  for  $D = 180, 240$  and  $300$  nm. Table 1 also summarizes these results. As can be seen,  $H_c^{\text{FORC}}$  increases from 420 to 760 Oe with increasing  $D$  from 180 to 300 nm at  $L_{\text{NM}} = 10$  nm, respectively.

In fact, the increase in  $D$  enhances both magnetizing- and demagnetizing-type interactions along the NW length and between neighboring NWs, respectively. This is reflected in the increase in the respective  $\Delta H_u$  from 1200 to 3000 Oe. For FM/NM multilayered NWs with reduced interactions (figures 5(d)–(f)) at  $L_{\text{NM}} = 140$  nm, larger  $D$  (300 nm) leads

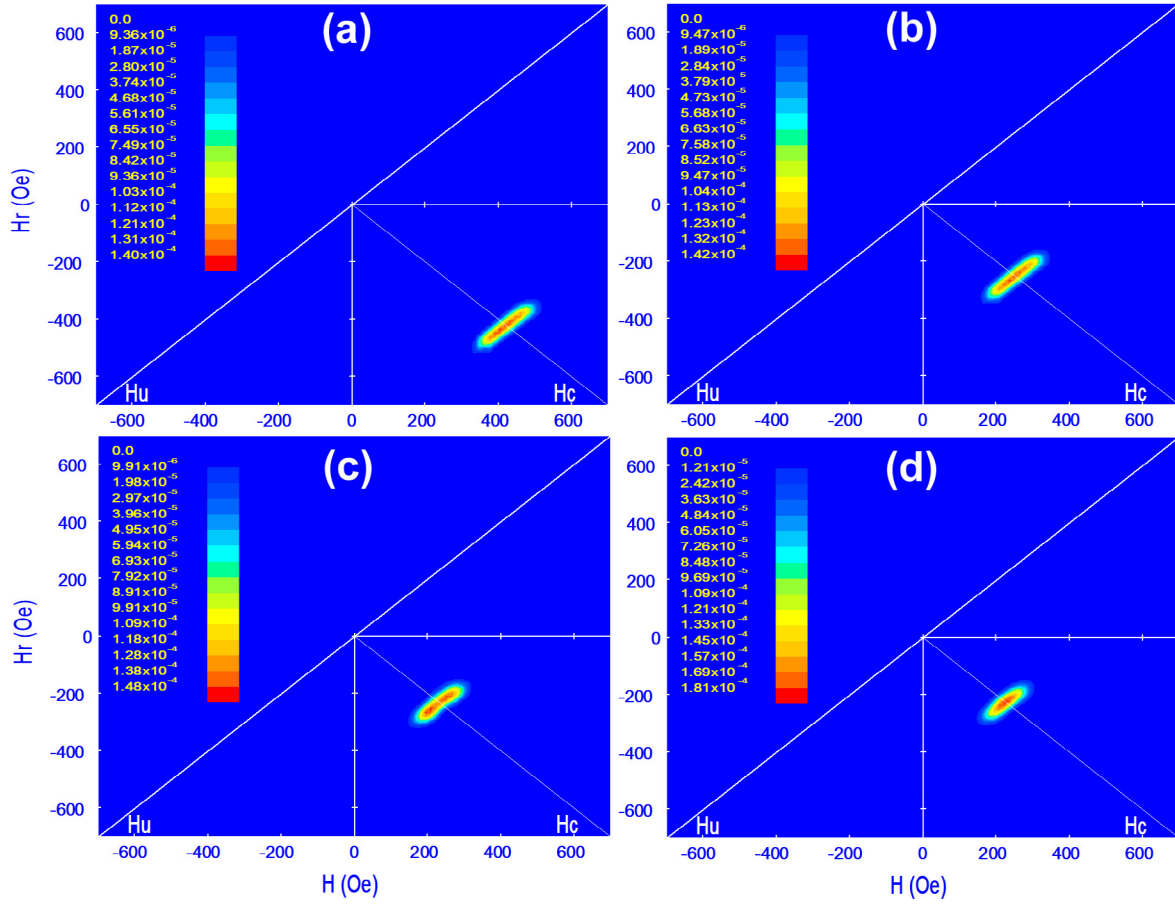


**Figure 8.** FORC diagrams of FM/NM multilayered NWs with  $L_{NM}$  of: (a) 10 nm (b) 60 nm, (c) 150 nm and (d) 300 nm at  $D = 180$  nm and  $d = 1000$  nm.

to a higher  $H_c^{FORC}$  (290 Oe) compared to that of  $D = 180$  nm ( $H_c^{FORC} = 245$  Oe).

### 3.3. The effect of interwire distance ( $d$ ) on FORC distribution

Figures 7(a)–(c) depict  $H_c^{FORC}$  of FM/NM multilayered NWs as a function of  $L_{NM}$  for different  $d$  (600–1000 nm) at  $D = 180$  nm. From figures 7(a) and (b), the comparison between typical, first and second features along with the corresponding  $H_c^{FORC}$  values shows almost the same behavior, except that the first feature differently disappears for  $L_{NM} \geq 140$  nm at  $d = 600$  nm.

Increasing  $d$  to 1000 nm, figure 7(c) indicates the elimination of the first and second features without a considerable change in the typical one in terms of  $H_c^{FORC}$  value. In fact, the parameter  $d$  can only influence the demagnetizing-type interwire interactions between multilayered NWs. Thus, the disappearance of the emerging features at  $d = 1000$  nm may be induced by a reduction in the demagnetizing-type interactions. In this case, FORC diagrams of the FM/NM NWs with  $L_{NM}$  10 nm, 60 nm, 150 nm and 300 nm depicted in figure 8 evidence a decrease in  $\Delta H_u$  when compared to each corresponding FORC diagrams in figure 2 at  $d = 500$  nm.

### 3.4. Total magnetostatic energy ( $E_{tot}$ ) calculations

To better understand the physics behind the observations in the FORC diagrams and the effects of  $D$  and  $d$  on  $H_c^{FORC}$  behavior, total magnetostatic energy ( $E_{tot}$ ) was calculated when the NW segments were magnetically saturated parallel to each other, and the results obtained are shown in figure 9. Figures 9(a) and (b) show the comparison between  $E_{tot}$  values of FM/NM multilayered NWs with  $d = 500$  nm as a function of  $L_{NM}$  for  $D = 180, 240$  and 300 nm, and the corresponding 3D surface plot, respectively. For each  $D$ , increasing  $L_{NM}$  shows a decreasing trend of  $E_{tot}$ , reducing it from positive to negative values. While positive  $E_{tot}$  is caused by dominant magnetizing-type interactions, negative  $E_{tot}$  reveals the presence of stronger demagnetizing- than magnetizing-type ones. For  $E_{tot} = 0$  erg, both types of interactions have the same strength.

From FORC diagrams (figure 2),  $\Delta H_u$  of the FM/NM multilayered NWs with constant  $D$  and  $d$  was found to decrease with increasing  $L_{NM}$ , indicating a reduction in magnetostatic interactions. This is in agreement with the magnetostatic energy evaluation whereby the demagnetizing-type magnetostatic interactions are continuously reduced as a function of  $L_{NM}$ . Moreover, the multilayered NWs reach  $E_{tot} = 0$  erg



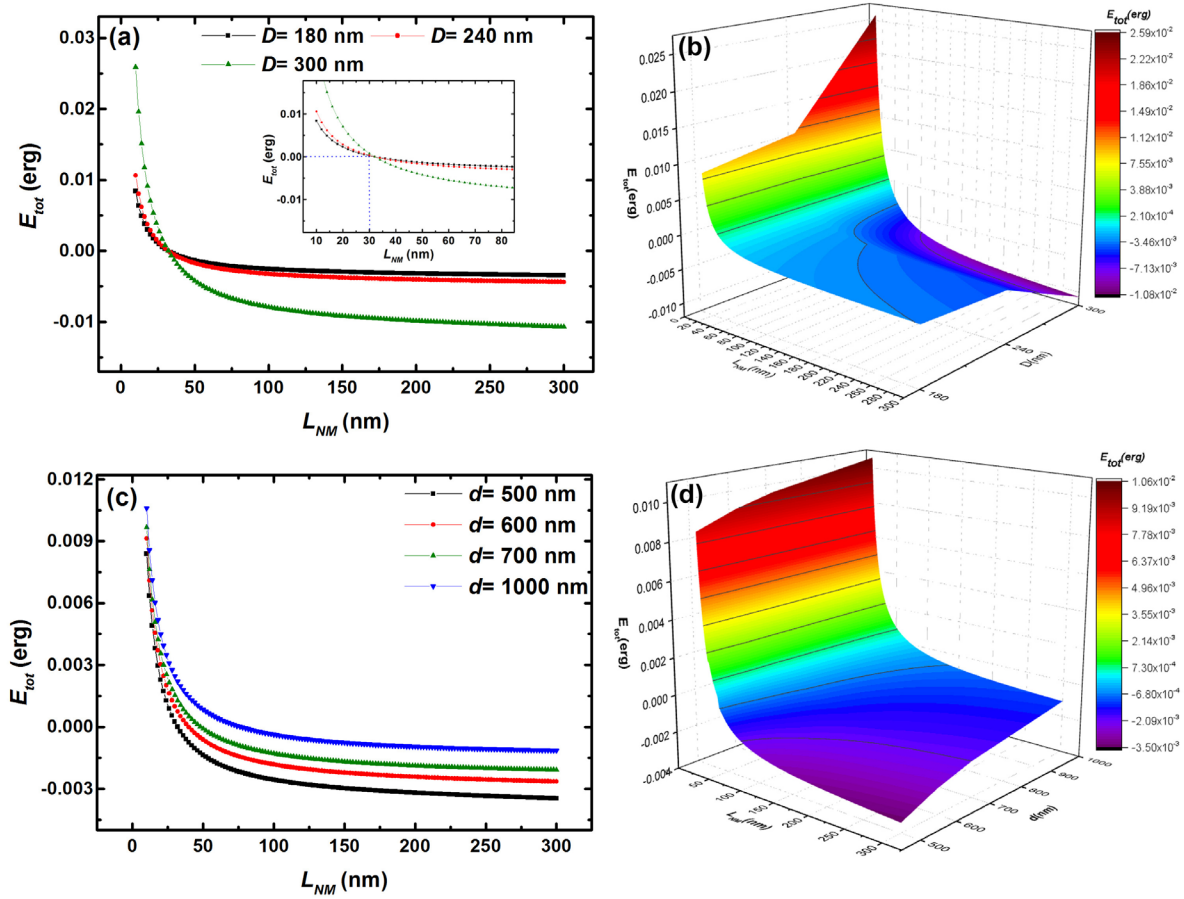


**Figure 9.** (a) The comparison between  $E_{\text{tot}}$  values of FM/NM multilayered NWs with  $d = 500$  nm as a function of  $L_{\text{NM}}$  for  $D = 180$ , 240 and 300 nm. (b) Corresponding 3D surface plot of panel (a). (c) The comparison between  $E_{\text{tot}}$  values of FM/NM multilayered NWs with  $D = 180$  nm as a function of  $L_{\text{NM}}$  for  $d = 500$ , 600, 700 and 1000 nm. (b) Corresponding 3D surface plot of panel (c). The inset in panel (a) highlights  $E_{\text{tot}} = 0$  erg for  $D = 180$  nm.

at very similar  $L_{\text{NM}}$ . With regard to coercive field behavior, the comparison between figures 6 and 9(a) shows that the decreasing trend of  $H_c^{\text{FORC}}$  with increasing  $D$  follows that of  $E_{\text{tot}}$ . As a result,  $H_c^{\text{FORC}}$  is reduced only by decreasing magnetizing-type interactions. For this reason,  $H_c^{\text{FORC}}$  of the FM/NM multilayered with larger  $D = 300$  nm remains higher than that of  $D = 180$  nm when  $E_{\text{tot}} \leq 0$  erg. On the other hand, the comparison between  $L_{\text{NM}}$  values obtained for  $E_{\text{tot}} = 0$  erg and the newly emerged features in respective FORC diagrams (see figure 2) reveals that  $H_c^{\text{FORC}}$  of the second feature separates from the typical one upon reaching negative  $E_{\text{tot}}$ . This has been marked by the dotted line in the insets of figures 3 and 9(a), specifying the role of prevalent demagnetizing-type interactions in inducing different FORC distributions.

$E_{\text{tot}}$  values and corresponding 3D surface plot of FM/NM multilayered NWs with  $D = 180$  nm as a function of  $L_{\text{NM}}$  for  $d = 500 - 1000$  nm are shown in figures 9(c) and (d), respectively. It is found that  $E_{\text{tot}}$  versus  $L_{\text{NM}}$  behavior of  $d = 500$ , 600 and 700 nm is similar to each other, changing from positive to negative values for  $L_{\text{NM}} > 30$ , 40 and 50 nm, respectively. The similarity found between  $E_{\text{tot}}$  versus  $L_{\text{NM}}$  behavior may indicate the presence of similar interactions affecting FM/NM NWs, leading to the almost the same  $H_c^{\text{FORC}}$  behavior of  $d = 500 - 700$  nm (figures 2, 7(a) and (b)). At  $d = 1000$  nm, increasing  $L_{\text{NM}}$  initially decreases  $E_{\text{tot}}$  and then maintains it

near zero value. This means that the prevalent interactions are magnetizing-type ones due to the large enough  $d$ , thus avoiding the FM/NM NW system to allow for the emergence of the first and second features (see figures 7(c) and 8).

#### 4. Conclusions

3D magnetic multilayered NW arrays with a constant  $L_{\text{FM}} = 6 \mu\text{m}$ , and respective  $L_{\text{NM}}$ ,  $D$  and  $d$  ranging between 10–300 nm, 180–300 nm and 500–1000 nm were simulated in hexagonally ordered anodic aluminum oxide templates using Monte Carlo calculations. The effects of  $L_{\text{NM}}$ ,  $D$  and  $d$  on FORC diagrams and distributions of interacting FM/NM NW arrays saturated in the parallel direction were thoroughly investigated. Increasing  $L_{\text{NM}}$  decreased both interwire and intrasegment interactions, leading to the emergence of the first feature (a pair distribution with positive and negative peaks) and the second feature (similar to the typical distribution of NW arrays) in the FORC diagrams for  $L_{\text{NM}} \geq 30$  nm. Meanwhile,  $H_c^{\text{FORC}}$  of all features showed a decreasing trend as a function of  $L_{\text{NM}}$ . Increasing  $D$  pushed the typical FORC distribution toward higher coercive fields while also enhancing both magnetizing- and demagnetizing-type interactions. The parameter  $d$  influenced only the demagnetizing-type interwire interactions between

multilayered NWs so that the emerging features disappeared at  $d = 1000$  nm. The variation behavior of  $E_{\text{tot}}$  followed that of  $H_c^{\text{FORC}}$  as a function of  $L_{\text{NM}}$  for different  $D$  and  $d$ , indicating a reduction in magnetostatic interactions.

## Acknowledgments

Institute of Nanoscience and Nanotechnology in University of Kashan is highly acknowledged for providing financial support to undertake this research by Grant No. (159023/58).

## ORCID iDs

A Ramazani  <https://orcid.org/0000-0003-4162-6600>

A H Montazer  <https://orcid.org/0000-0003-0629-0259>

## References

- [1] Binasch G, Grünberg P, Saurenbach F and Zinn W 1989 Enhanced magnetoresistance in layered magnetic structures with antiferromagnetic interlayer exchange *Phys. Rev. B* **39** 4828
- [2] Li M, Cui W, Yu J, Dai Z, Wang Z, Katmis F, Guo W and Moodera J 2015 Magnetic proximity effect and interlayer exchange coupling of ferromagnetic/topological insulator/ferromagnetic trilayer *Phys. Rev. B* **91** 014427
- [3] Wang Z and Victora R 2016 Enhancement of giant magnetoresistance and oscillation by wave-vector filtering in Fe/Ag/Fe/InAs/Ag *Phys. Rev. B* **94** 245415
- [4] Haldar A, Kumar D and Adeyeye A O 2016 A reconfigurable waveguide for energy-efficient transmission and local manipulation of information in a nanomagnetic device *Nat. Nanotechnol.* **11** 437
- [5] Wang X, Parkin S and Xue Q-K 2016 Preface to special topic: 2D spintronics *APL Mater.* **4** 032201
- [6] Vidal-Silva N, Tejo F, Espejo A and Escrig J 2019 Current-driven domain wall motion in a planar nanowire with a square hole *J. Magn. Magn. Mater.* **484** 114–9
- [7] Shiroyama T, Sakuraba Y, Nakatani T, Sepehri-Amin H, Jung J and Hono K 2018 High magnetic field sensitivity in anti-ferromagnetically coupled 001-epitaxial [Co<sub>2</sub>Fe (Al<sub>0.5</sub>Si<sub>0.5</sub>)/Ag] N multilayers *J. Appl. Phys.* **124** 163910
- [8] Martinez-Boubeta C, Ferrante Y and Parkin S 2015 Magnetotransport properties of spin-valve structures with Mg spacer layers *Appl. Phys. Lett.* **106** 032412
- [9] Kabanov Y P, Nikitenko V, Tikhomirov O, Egelhoff W, Shapiro A and Shull R 2009 Unexpectedly long-range influence on thin-film magnetization reversal of a ferromagnet by a rectangular array of FeMn pinning films *Phys. Rev. B* **79** 144435
- [10] Kurebayashi H, Dzyapko O, Demidov V E, Fang D, Ferguson A J and Demokritov S O 2011 Controlled enhancement of spin-current emission by three-magnon splitting *Nat. Mater.* **10** 660
- [11] Fullerton E E and Schuller I K 2007 The 2007 Nobel Prize in physics: magnetism and transport at the nanoscale *ACS Nano* **5** 384–9
- [12] Cox B, Davis D and Crews N 2013 Creating magnetic field sensors from GMR nanowire networks *Sensors Actuators A* **203** 335–40
- [13] Sergelius P, Lee J H, Fruchart O, Salem M S, Allende S, Escobar R A, Gooth J, Zierold R, Toussaint J-C and Schneider S 2017 Intra-wire coupling in segmented Ni/Cu nanowires deposited by electrodeposition *Nanotechnology* **28** 065709
- [14] Böhnert T, Niemann A C, Michel A-K, Bäßler S, Gooth J, Tóth B G, Neuróhr K, Péter L, Bakonyi I and Vega V 2014 Magnetothermopower and magnetoresistance of single Co-Ni/Cu multilayered nanowires *Phys. Rev. B* **90** 165416
- [15] Lopatin S, Ivanov Y P, Kosel J and Chuvilin A 2018 TEM study of current-induced domain wall motion in cylindrical nanowires: towards 3D magnetic memory devices *Microsc. Microanal.* **24** 944–5
- [16] Ivanov Y P, Chuvilin A, Lopatin S and Kosel J 2016 Modulated magnetic nanowires for controlling domain wall motion: toward 3D magnetic memories *ACS Nano* **10** 5326–32
- [17] Ivanov Y P and Chubykalo-Fesenko O 2015 Micromagnetic simulations of cylindrical magnetic nanowires *Magnetic Nano-and Microwires* (New York: Elsevier) pp 423–48
- [18] Zhang J, Ma H, Zhang S, Zhang H, Deng X, Lan Q, Xue D, Bai F, Mellors N J and Peng Y 2015 Nanoscale characterisation and magnetic properties of Co<sub>81</sub> Cu<sub>19</sub>/Cu multilayer nanowires *J. Mater. Chem. C* **3** 85–93
- [19] Ramazani A, Ghaffari M, Kashi M A, Kheiry F and Eghbal F 2014 A new approach to fabricating magnetic multilayer nanowires by modifying the ac pulse electrodeposition in a single bath *J. Phys. D: Appl. Phys.* **47** 355003
- [20] Salem M S, Tejo F, Zierold R, Sergelius P, Moreno J M M, Goerlitz D, Nielsch K and Escrig J 2018 Composition and diameter modulation of magnetic nanowire arrays fabricated by a novel approach *Nanotechnology* **29** 065602
- [21] Moraes S, Navas D, Béron F, Proenca M, Pirota K, Sousa C and Araújo J 2018 The role of Cu length on the magnetic behaviour of Fe/Cu multi-segmented nanowires *Nanomaterials* **8** 490
- [22] Tehrani A S, Kashi M A, Ramazani A and Montazer A 2016 Axially adjustable magnetic properties in arrays of multilayered Ni/Cu nanowires with variable segment sizes *Superlattices Microstruct.* **95** 38–47
- [23] Susano M, Proenca M, Moraes S, Sousa C and Araújo J 2016 Tuning the magnetic properties of multisegmented Ni/Cu electrodeposited nanowires with controllable Ni lengths *Nanotechnology* **27** 335301
- [24] Kashi M A, Ramazani A and Esmaeili A 2013 Magnetostatic interaction investigation of CoFe alloy nanowires by first-order reversal-curve diagrams *IEEE Trans. Magn.* **49** 1167–71
- [25] Béron F, Carignan L-P, Ménard D and Yelon A 2008 Magnetic behavior of Ni/Cu multilayer nanowire arrays studied by first-order reversal curve diagrams *IEEE Trans. Magn.* **44** 2745–8
- [26] Arzuza L, López-Ruiz R, Salazar-Aravena D, Knobel M, Béron F and Pirota K 2017 Domain wall propagation tuning in magnetic nanowires through geometric modulation *J. Magn. Magn. Mater.* **432** 309–17
- [27] Béron F, Clime L, Ciureanu M, Ménard D, Cochrane R and Yelon A 2008 Magnetostatic interactions and coercivities of ferromagnetic soft nanowires in uniform length arrays *J. Nanosci. Nanotechnol.* **8** 2944–54
- [28] Nica M and Stancu A 2015 FORC diagram study of magnetostatic interactions in 2D longitudinal arrays of magnetic wires *Physica B* **475** 73–9
- [29] Rando E and Allende S 2015 Magnetic reversal modes in multisegmented nanowire arrays with long aspect ratio *J. Appl. Phys.* **118** 013905
- [30] Dobrota C-I and Stancu A 2013 What does a first-order reversal curve diagram really mean? A study case: array of ferromagnetic nanowires *J. Appl. Phys.* **113** 043928
- [31] Dobrota C-I and Stancu A 2015 Tracking the individual magnetic wires' switchings in ferromagnetic nanowire

- arrays using the first-order reversal curves (FORC) diagram method *Physica B* **457** 280–6
- [32] Béron F, Pirota K R, Vega V, Prida V, Fernández A, Hernando B and Knobel M 2011 An effective method to probe local magnetostatic properties in a nanometric FePd antidot array *New J. Phys.* **13** 013035
- [33] Palmero E M, Béron F, Bran C, del Real R P and Vázquez M 2016 Magnetic interactions in compositionally modulated nanowire arrays *Nanotechnology* **27** 435705
- [34] Pike C, Ross C, Scalettar R and Zimanyi G 2005 First-order reversal curve diagram analysis of a perpendicular nickel nanopillar array *Phys. Rev. B* **71** 134407
- [35] Proenca M, Ventura J, Sousa C, Vazquez M and Araujo J 2014 Angular first-order reversal curves: an advanced method to extract magnetization reversal mechanisms and quantify magnetostatic interactions *J. Phys.: Condens. Matter* **26** 116004
- [36] Almasi-Kashi M, Ramazani A, Izadi S and Jafari-Khamse E 2015 Correlation between microstructure and first-order-reversal-curve of Co nanowire arrays *Phys. Scr.* **90** 085803
- [37] Wong J, Greene P, Dumas R K and Liu K 2009 Probing magnetic configurations in Co/Cu multilayered nanowires *Appl. Phys. Lett.* **94** 032504
- [38] Béron F, Ménard D and Yelon A 2008 First-order reversal curve diagrams of magnetic entities with mean interaction field: a physical analysis perspective *J. Appl. Phys.* **103** 07D908
- [39] Dobrota C-I and Stancu A 2012 Mean field model for ferromagnetic nanowire arrays based on a mechanical analogy *J. Phys.: Condens. Matter* **25** 035302
- [40] Ruta S, Hovorka O, Huang P-W, Wang K, Ju G and Chantrell R 2017 First order reversal curves and intrinsic parameter determination for magnetic materials; limitations of hysteron-based approaches in correlated systems *Sci. Rep.* **7** 45218
- [41] Gilbert D A, Zimanyi G T, Dumas R K, Winklhofer M, Gomez A, Eibagi N, Vicent J and Liu K 2014 Quantitative decoding of interactions in tunable nanomagnet arrays using first order reversal curves *Sci. Rep.* **4** 4204
- [42] Pike C and Fernandez A 1999 An investigation of magnetic reversal in submicron-scale Co dots using first order reversal curve diagrams *J. Appl. Phys.* **85** 6668–76
- [43] Muxworthy A, Heslop D and Williams W 2004 Influence of magnetostatic interactions on first-order-reversal-curve (FORC) diagrams: a micromagnetic approach *Geophys. J. Int.* **158** 888–97
- [44] Choi J, Sauer G, Nielsch K, Wehrspohn R B and Gösele U 2003 Hexagonally arranged monodisperse silver nanowires with adjustable diameter and high aspect ratio *Chem. Mater.* **15** 776–9
- [45] Sun L, Hao Y, Chien C-L and Searson P C 2005 Tuning the properties of magnetic nanowires *IBM J. Res. Dev.* **49** 79–102
- [46] Laroze D, Escrig J, Landeros P, Altbir D, Vázquez M and Vargas P 2007 A detailed analysis of dipolar interactions in arrays of bi-stable magnetic nanowires *Nanotechnology* **18** 415708
- [47] Karpuz A, Kockar H and Alper M 2014 Study of electrolyte pH in production of Cu–Co–Ni ternary alloys and its effect on microstructural and magnetic properties *IEEE Trans. Magn.* **50** 1–4